Modeling colliding beams with an element by element representation of the storage ring guide field

D. L. Rubin, S. Isaacman, and A. Long

Laboratory of Elementary Particle Physics, Cornell University, Ithaca, New York 14853, USA
(Received 9 May 2005; published 26 January 2006)

A detailed model of the Cornell Electron Storage Ring (CESR) guide field, including beam-beam interaction computed in the weak-strong regime, is the basis for a multiturn simulation of luminosity. The simulation reproduces the dependence of luminosity on bunch current that is measured in the storage ring, at both high-energy (5.3 GeV/beam) and in the wiggler-dominated low energy (CESR-*c*) configuration (1.9 GeV/beam). Dynamics are determined entirely by the physics of propagation through the individual guide field elements with no free parameters. Energy dependence of the compensation of the transverse coupling introduced by the experimental solenoid is found to significantly degrade specific luminosity. The simulation also indicates a strong dependence of limiting beam-beam tune shift parameter on the geometric mean of synchrotron tune and bunch length.

I. INTRODUCTION

We have developed a simulation of the dynamics of colliding beams in the Cornell Electron Storage Ring (CESR), that determines equilibrium beam size and luminosity, and is based on a detailed model of the ring guide field. CESR operates with counter-rotating beams in a single vacuum chamber. Electrostatic deflectors differentially distort the closed orbits of the electrons and positrons. The temporal spacing of the bunches in each beam is chosen so that at the multiple crossing points the closed orbits are separated in the horizontal plane. With nine trains of five bunches in each beam, each bunch of electrons is witness to 89 near misses with a positron bunch in each revolution of the storage ring. Within each train, bunches are spaced 14 ns apart [1].

In order to reproduce as realistically as possible the effects of the guide field nonlinearities, the ring is described in terms of the complete sequence of machine elements. At each of the parasitic crossing points, a beam-beam element is included to model the effect of the bunch in the strong beam on the weak beam macroparticles. The fields of the superconducting damping wiggler magnets are represented as analytic functions fitted to a field table generated by a finite element code [2]. Tracking is based on symplectic integration [3].

The beam-beam interactions are computed in the weak-strong regime, assuming a Gaussian distribution of charge in the strong bunch. The weak-strong approximation is valid as long as the bunch current is below the threshold for coherent motion of colliding bunches, and the distribution of the charge in the weak bunch remains Gaussian. For CESR parameters we find that the lifetime limiting current

is below the threshold for coherent effects of the beam-beam interaction.

The equilibrium beam sizes are determined by the statistical emission of photons in all bending fields, damping imposed by the rf acceleration, optical functions, and beam-beam interaction. There are no free parameters in the model, and the simulation yields an absolute prediction of dependence of luminosity on bunch current. We find excellent agreement of model predictions and measurement of luminosity for colliding beams at 5.3 GeV/beam and also in the wiggler-dominated low energy configuration of CESR (CESR-*c*) at 1.9 GeV/beam.

There is no new *physics* in the model. Our emphasis on the details of the dynamics of the arc guide field is intended to identify features relevant to beam-beam performance. The simulations indicate that wiggler nonlinearities, parasitic crossings, and the small crossing angle have negligible effect on the limiting beam-beam tune shift. We rather find sensitivity to the energy dependence of the solenoid compensation and to bunch length and synchrotron tune.

II. WEAK-STRONG VS STRONG-STRONG BEAM-BEAM MODEL

In the weak-strong model, the strong beam is fixed in space and its charge distribution is Gaussian in three dimensions, two transverse and one longitudinal. The parameters of the Gaussian are initialized by an analytic determination of the single beam equilibrium size. Beginning after one damping time, the weak beam particle distribution is fitted to a Gaussian every 500 turns, and its size compared to the strong beam. The strong beam size is updated for self-consistency as required. After several damping times either the beams reach equilibrium, or particles are lost.

---

*Electronic address: drubin@physics.cornell.edu

If the beam sizes do not come to equilibrium, or if the weak beam distribution cannot be well described by a Gaussian, as measured by the quality of the fit, then this implementation of the weak-strong approximation has evidently lost its validity. Since the strong beam is fixed in space, coherent motion of the colliding bunches is artificially excluded.

The advantage of the weak-strong approximation over the strong-strong simulation is that many fewer macroparticles need to be tracked. Because the distribution of particles in the strong-strong simulations is unconstrained, a relatively large number of macroparticles is necessary to properly represent the bunches, and that number limits the speed of calculation. In strong-strong models, the dynamics are assumed dominated by the beam-beam interaction, and the machine arc guide field is typically modeled as a map of finite order. Sophisticated models of the beam-beam interaction have been developed [4–7] and the associated simulations can exhibit coherent motion of the beams and flip-flop of beam size, phenomena clearly excluded in a weak-strong model. But in the current regime relevant to CESR-c operation, we find that the weak-strong approximation includes the essential physics of the beam-beam interaction.

Insofar as our objective is to explore the effects of single particle dynamics on luminosity, we neglect the single beam collective effects that are included in strong-strong codes like ODYSSEUS [7]. With dipole feedback operating in horizontal, vertical and longitudinal planes the measured instability threshold at 1.9 GeV/beam energy is nearly 3 times the beam-beam limited current [8]. We anticipate that collective effects can reasonably be ignored at the relatively low current at which CESR-c operates.

In CESR-c the electron and positron closed orbits are electrostatically separated with typically 89 long range beam-beam interactions distributed throughout the machine arc, and off-axis in most of the guide field sextupoles. The sources of synchrotron radiation are highly localized [9]. The damping wigglers impose a strong vertical cubic nonlinearity, and though they extend over only 2% of the machine circumference, they are responsible for 90% of the synchrotron radiation. Finally, in the interaction region, the beams collide with a small crossing angle.

In view of the complexity of the transport through the arc we choose to represent it as precisely as possible, as a sequence of the individual elements. At low current, the luminosity is dominated by the physics of the machine arcs, rather than by the beam-beam interaction. Furthermore, we find that the measured beam-beam limiting current is approximately the same as the limit of validity of the weak-strong model. We conclude that the weak-strong simulation can be used to explore the dependence of the size and distribution of the macroparticles in the weak beam on the lattice functions, parasitic interactions, orbits, and guide field nonlinearities.

III. PHYSICS OF THE SIMULATION

A. Machine model

The model of the machine guide field, including all magnetic, electrostatic, and components, is constructed with BMAD [3] subroutines and data structures. In the interaction region, quadrupoles and skew quadrupoles are inside the field of the CLEO solenoid. The mapping for the superimposed fields is based on a transport matrix for their linear combination. Sextupoles are represented as a series of thin kicks. The third order map for the damping wigglers is based on an analytic fit to a field table generated by a finite element code. [2] The accelerating field is sinusoidal. Each of these elements can be further modified by arbitrary offsets, tilts, and field errors. Tracking through the elements is 6-dimensional and symplectic [3].

B. Radiation damping and fluctuations

Damping and quantum excitation is treated on an element by element basis. We determine the average synchrotron radiation energy loss, U_0, and a probabilistic energy fluctuation, u, twice in each element, once on entry and again on exit. The average fractional energy loss is

$$\frac{U_0}{E} = \frac{2}{3} r_e \gamma^3 G^2 l, \tag{1}$$

where $G = 1/\rho$, r_e is the classical electron radius, E is the beam energy, and l is the length of the element. The distribution of energy fluctuations is Gaussian with standard deviation [10]

$$\sigma^2 = \frac{55}{24\sqrt{3}} u_c U_0 \tag{2}$$

and

$$u_c = \frac{3}{2} \hbar c \gamma^3 G \tag{3}$$

is the critical photon energy.

C. Beam-beam interaction

The simulation is weak-strong with particle distribution of the fixed beam assumed Gaussian in x-y-z. We use the Bassetti, Erskine [11] formulation to compute the kick of strong beam on macroparticles of the weak beam. The fixed beam is represented as two dimensional slices in the x-y plane distributed over the length of the bunch. The kick depends on bunch cross section, length, and charge. The dynamic beam consists of N macroparticles with Gaussian initial distribution. Macroparticles are then tracked individually and the turn by turn distribution is unconstrained.

D. Parasitic beam-beam interactions

The parasitic beam-beam kick is based on the same 2D beam-beam element as the main beam-beam interaction,

but with a single slice. At the "s" location of the parasitic crossing, the guide field element is split and a beam-beam element inserted. The x offset and y offset of the element correspond to the x and y coordinates of the closed orbit of the fixed beam.

E. Crossing angle

The horizontal and vertical pitch of the beam-beam element are set equal to the horizontal and vertical angles of the closed orbit of the fixed beam at the IP. The horizontal and vertical offsets correspond to horizontal and vertical position of the fixed beam closed orbit. The number of slices is chosen by the user. We use the simulation to determine the appropriate number of slices. For the typical CESR crossing angle of ± 3.5 mrad, we find that five slices is sufficient, as the dependence on the number of slices saturates with five.

F. Self-consistent weak-strong

The orientation of the strong beam at the interaction point coincides with the closed orbit of the beam and it is fixed. The initial beam size is computed analytically and depends in general on radiation integrals and coupling parameters. Beginning after one transverse damping time ($\sim 20\,000$ turns at 1.89 GeV and $\sim 10\,000$ turns at 5.3 GeV) the x-y-z distributions of the macroparticles in the weak beam are fit to Gaussians every 500 turns. The size of the fixed beam is updated to coincide with the size of the weak beam as required. The tilt, offsets, and pitches of the fixed beam are not changed.

We compute luminosity by summing the contribution from each of the macroparticles in the weak bunch. The calculation of luminosity assumes that the strong beam has a Gaussian distribution but makes no assumption about the weak beam distribution.

G. Initialization and tuning of model parameters

The simulation code permits adjustment of a variety of model parameters. The attributes of any of the machine elements, including quadrupole, skew quadrupole, sextupole magnets, separators, and cavities, can be initialized as desired to explore dependencies. β functions, dispersion, coupling, tunes, chromaticity, etc., can be adjusted as long as the relevant control group is defined in the lattice. The control group alters a family of machine elements to effect the change in the same way that the lattice parameters are tuned in the machine. Betatron and synchrotron tunes, and chromaticity are input parameters.

In the most basic initialization:

(i) Betatron tunes are set a safe distance from the half-integer and coupling resonance so that subsequent manipulations do not lead to instability.

(ii) Two dimensional beam-beam elements are introduced into the ring at the location of parasitic crossings for the specified bunch pattern and bunch current. The offsets correspond to the closed orbit of the strong beam.

(iii) A sliced beam-beam element is added to the ring at the interaction point with orientation coincident with the closed orbit of the strong beam and size based on emittance and optical parameters computed analytically for the strong beam.

(iv) The synchrotron tune is set to the desired operating point by adjustment of the accelerating voltage.

(v) The horizontal separator voltages are adjusted so that the difference in horizontal displacements of the closed orbits of weak and strong beam is zero at the interaction point. The closed orbit of the weak beam depends on the bunch current in the strong beam. Therefore, the separator voltages that bring beams into collision, also depend on bunch current.

(vi) The vertical separator voltages and vertical betatron phase advance between them (nominally 180°) are adjusted so that the vertical closed orbits of the two beams are coincident at the IP

(vii) The beam-beam element at the IP is turned off and the betatron tunes of the weak beam are set to the operating point. Note that the effect of the long range beam-beam kicks is included at this step.

(viii) Collision assurance is repeated and the tunes are reset as required.

(ix) The beam-beam element at the IP is restored.

(x) Tracking begins.

IV. CONVERGENCE

A. Number of turns

Beams converge to equilibrium sizes in about five radiation damping times. Figure 1 shows fitted vertical beam size of the weak bunch at the interaction point as a function of turn number. The machine configuration corresponds to CESR-c operation with 12 damping wigglers at 2.1 T peak field and 1.89 GeV beam energy, and nine 4-bunch trains in each beam. The radiation damping time is about 20 000 turns. Evolution of horizontal and longitudinal bunch sizes at the IP are shown in Figs. 2 and 3. The horizontal and longitudinal equilibrium beam sizes are very nearly independent of the bunch current. The vertical distribution has a significant current dependence that is evidently due to the beam-beam interaction.

Finally we show luminosity as a function of turn number in Fig. 4. Equilibrium is achieved in less than 10^5 turns. The size of the strong beam is updated to coincide with the fitted size of the weak beam beginning after one damping time, thus the step in luminosity at 20 000 turns.
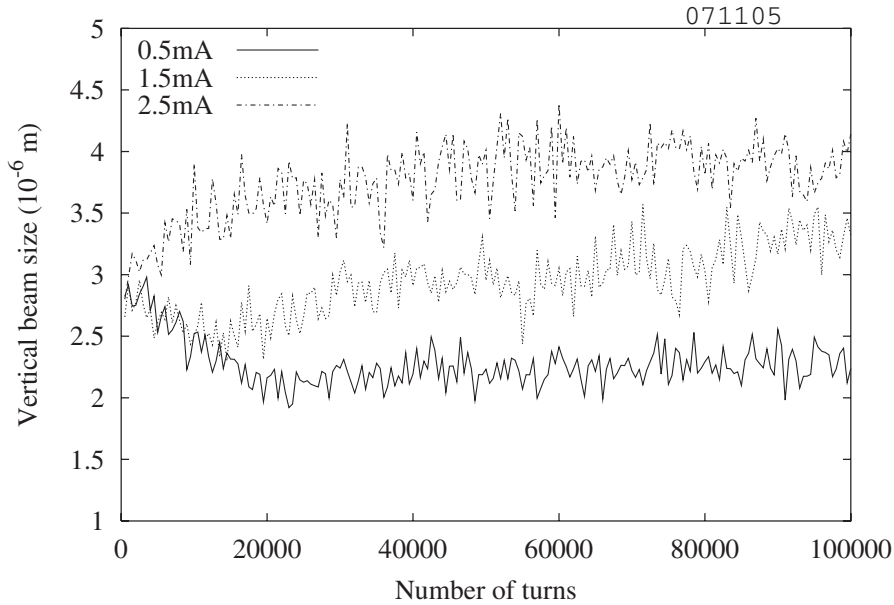
FIG. 1.   Fitted vertical size of the weak beam distribution at the interaction point vs number of turns for several bunch currents.

B. Number of macroparticles

Luminosity as a function of number of weak beam macroparticles is shown in Fig. 5. We see that 500 macroparticles adequately represent the weak beam distribution. Increasing the number of macroparticles beyond 500 does not significantly change the result. Convergence of luminosity with turn number for various numbers of macroparticles is shown in Fig. 6.

Turn by turn fluctuations shrink with an increasing number of particles. We define the uncertainty in the luminosity as the standard deviation of the average of the last 20 000 turns.

V. COMPARISON WITH MEASUREMENTS

We compare simulation and measurement of luminosity for two very different configurations of CESR, operation at 5.289 GeV/beam, and at 1.89 GeV/beam. In addition to the energy difference, the machine configurations are distinguished by: the interaction region optics, the CLEO solenoid field, and the introduction of damping and emittance wigglers for low energy operation. The highest specific luminosity is achieved only after extensive tuning of coupling, orbits, focusing parameters at the interaction point, and betatron tunes. For both data sets, the measurements were taken after many months of tuning had estab-
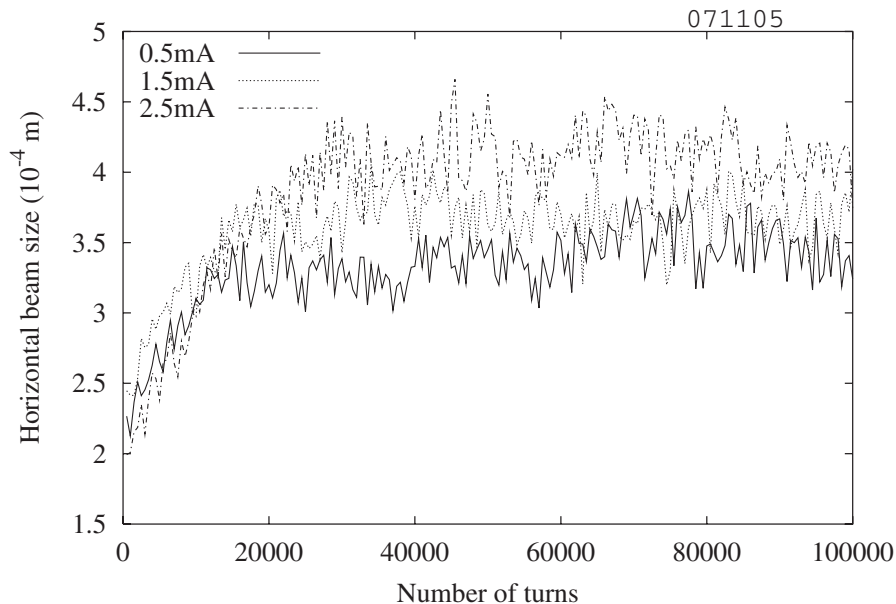

FIG. 2.   Fitted horizontal size of the weak beam distribution at the interaction point vs number of turns for several bunch currents.
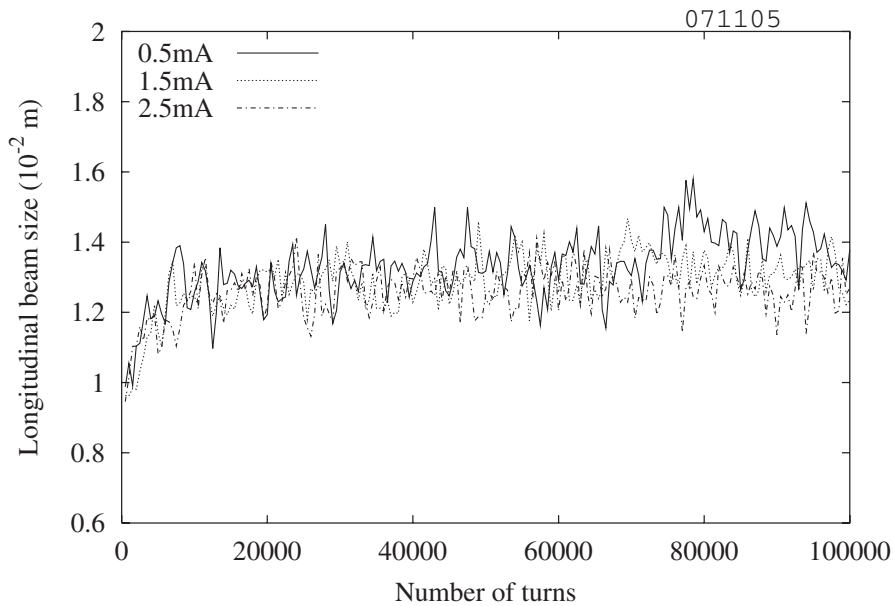
FIG. 3.   Fitted longitudinal size of the weak beam distribution at the interaction point vs number of turns for several bunch currents.

lished optimum performance, and in both cases there is good agreement between measured and calculated current dependence of luminosity.

A. 5.289 GeV/beam

The high-energy optics are based on the phase II interaction region and can accommodate nine trains of bunches in each beam with 4 bunches/train [1]. Bunches within the train are spaced every 14 ns. Trains are equally spaced every ∼280 ns. The horizontal crossing angle at the interaction point is ±2.4 mrad. The phase II interaction region

optics consist of a 1.5 m long vertically focusing permanent magnet with near end 60 cm from the IP. The permanent magnet is immersed in the 1.5 T field of the experimental solenoid. Immediately outside the solenoid return iron is a normally conducting, horizontally focusing quadrupole. A third large aperture, but relatively weak, vertically focusing quadrupole is about 6 m from the IP and provides the necessary energy reach. The three quadrupoles are rotated by 4.33°, 6.23°, and 12.6°, respectively, to compensate the coupling introduced by the solenoid. The linear lattice [12] is designed to optimize the effective
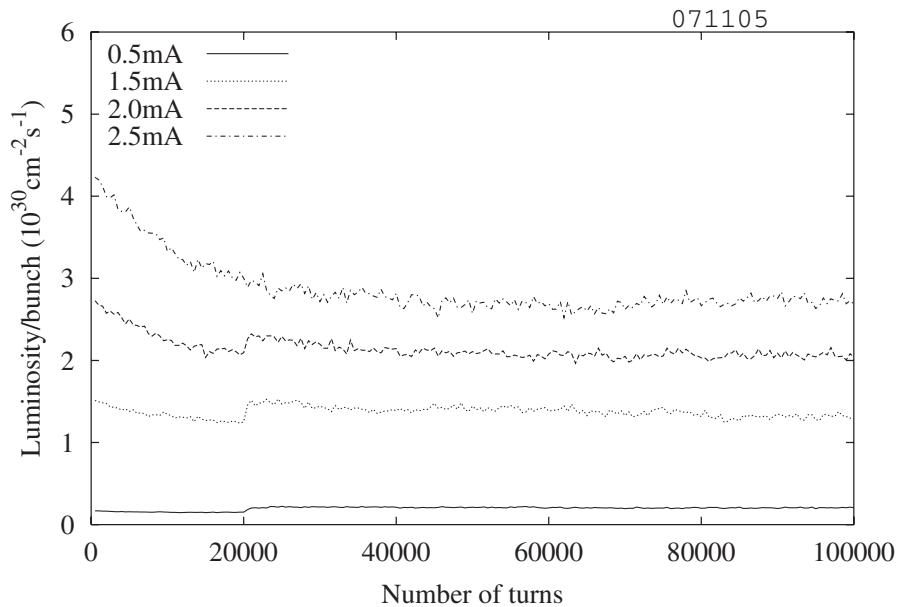

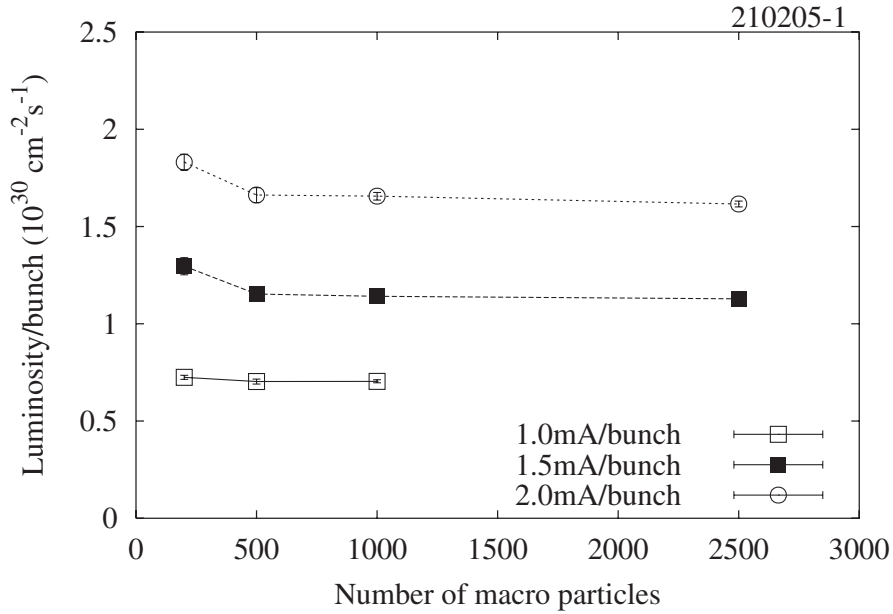FIG. 4.   Luminosity computed every 500 turns versus turn number for various bunch currents.

FIG. 5.   Luminosity as a function of number of weak beam macroparticles for various bunch currents.

separation of the counter-rotating bunches at the 71 parasitic crossing points and to yield the optical parameters summarized in Table I. The typical horizontal separation of bunches at the parasitic crossings is 7–10 σ_x. The sextupole distribution minimizes energy and amplitude dependence of β functions, and establishes chromaticity near unity. The measured and simulated dependence of luminosity on bunch current is shown in Fig. 7. The single bunch luminosity data is the average of the total measured luminosity for 36 bunches. In the simulation, there are 36 bunches in the strong beam and we compute the luminosity

for the single weak beam bunch. The agreement is excellent. Note that there are no free parameters in the calculation. The beam size is derived from the equilibrium distribution due to radiation in the bending fields, energy dependence of closed orbit, β^* and coupling, and beam-beam effects.

B. 1.89 GeV

CESR operates at low energy (1.89 GeV/beam) with the phase III [13] final focus and 12 1.3 m long, 2.1 T wigglers
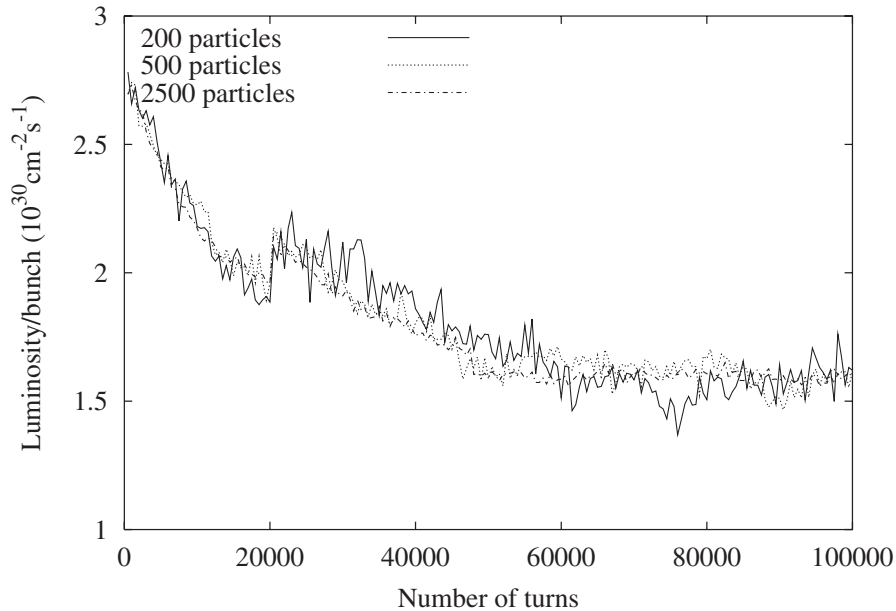

FIG. 6.   Luminosity at 2 mA/bunch as a function turn number for different numbers of macroparticles.

TABLE I.   Parameters of high-energy optics, low energy optics with 12 2.1 T wigglers and low energy optics with no damping wigglers.

Parameter	High-energy	Low energy 12 wiggler	Low energy 0 wigglers
Energy [GeV]	5.289	1.89	1.89
Q_h	10.534	10.532	10.532
Q_v	9.594	9.594	9.594
Q_s	0.05	0.089	0.049
β_v^* [mm]	18	12	12
β_h^* [cm]	95	84	84
σ_l [mm]	19	13.2	6.2
τ_h [ms]	23.5	49.6	556.4
ϵ_h [nm]	205	128	20.5
σ_E/E [%]	0.678	0.843	0.222
Bunch trains	9	8	8
Bunches/train	4	5	5

installed in the machine arcs. The wigglers reduce the radiation damping time and increase horizontal emittance [9]. The storage ring is wiggler dominated, with ~90% of synchrotron radiation emitted in the 15.6 m of wiggler that corresponds to ~2% of the ring circumference. The final focus consists of a 20 cm long permanent magnet quadrupole 30 cm from the IP, and then a pair of vertical and horizontally focusing superconducting quadrupoles centered 1.16 m and 2.08 m from the IP, respectively. All three of the interaction region quadrupoles are rotated 4.5° about their axes, and skew quad windings are superimposed on

the superconducting pair to fine tune coupling compensation of the 1T experimental solenoid.

The lattice is designed to accommodate nine 5-bunch trains of counter-rotating bunches. The lattice parameters are summarized in Table I. Note the longer damping time and increased energy spread with respect to the high-energy optics. Also, the phase III final focus yields smaller β^* than phase II. Sextupoles are optimized as for the high-energy optics except that the nonneglible sextupole component of the wigglers is included in the determination of chromaticity and energy dependence of β.
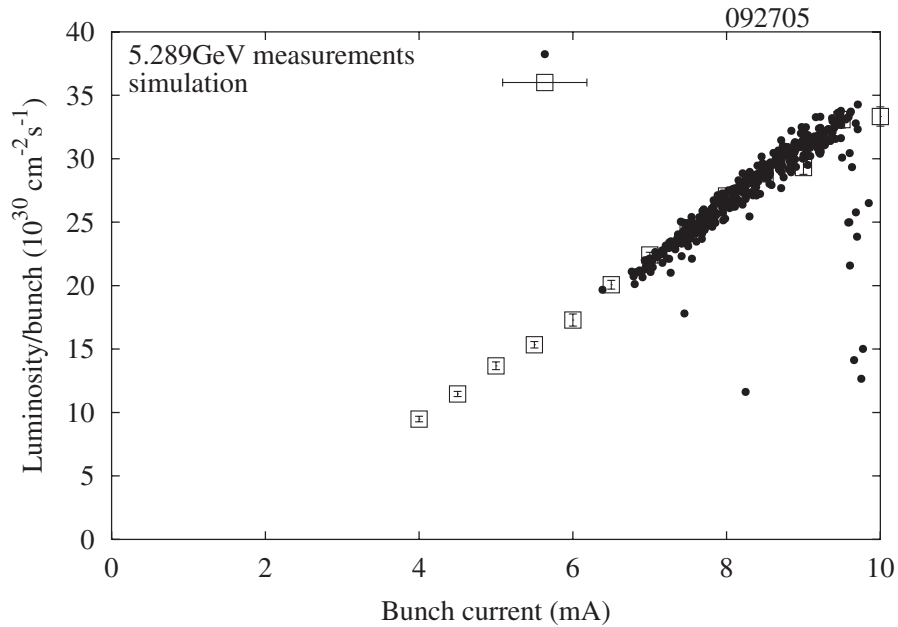

FIG. 7.   The measured luminosity points are collected once every 3 min over the 24 h period during which the highest specific luminosity was achieved in the high-energy configuration, March 3, 2001. The simulation is with 500 macroparticles and 100 000 turns.
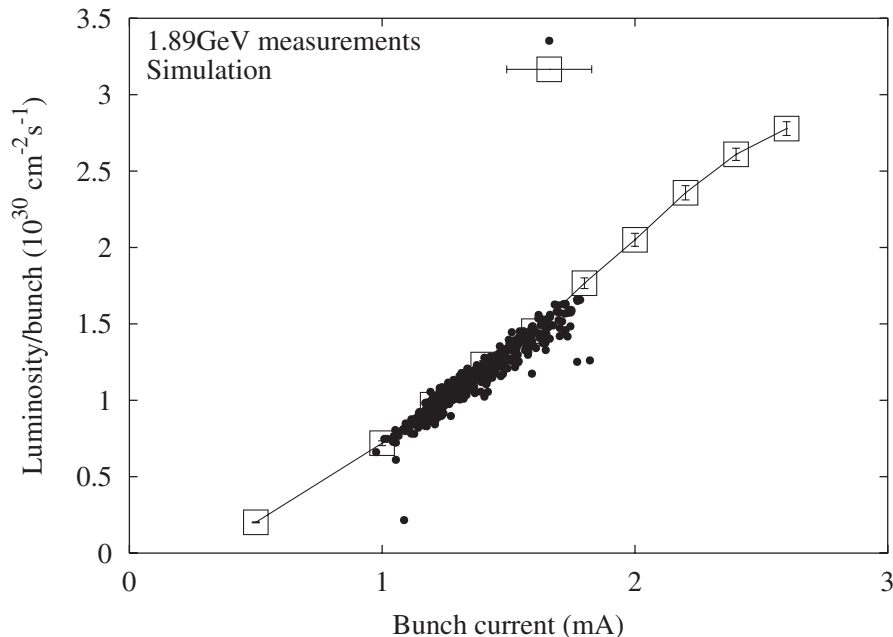
FIG. 8.   The measured luminosity points are collected once every 3 min over the 24 h period during which the highest specific luminosity was achieved in the low energy (CESR-*c*) configuration, October 30, 2004. The simulation is based on tracking 500 macroparticles through 10^5 turns.

The measured and simulated dependence of luminosity on bunch current are shown in Fig. 8. The single bunch luminosity data is the average of the total measured luminosity for 40 bunches.[1] Again the measurements are in good agreement with the simulation.

Like machine tunes, simulation tunes are chosen empirically to maximize performance. A map of simulated luminosity on the tune plane for the CESR-*c* 12 wiggler configuration is shown in Fig. 9. The grid points in the plot correspond to the tunes of the weak beam, including effects of parasitic interactions, and excluding the main beam-beam collision. While the tune so defined is straightforward to calculate, it is difficult to measure directly. To the extent that the corresponding tunes can be measured, the tunes that yield optimum measured and computed luminosity are consistent. For this configuration we find maximum luminosity when $Q_x = 0.527$ and $Q_y = 0.586$. The synchrotron tune is $Q_s = 0.089$.

VI. VALIDITY OF THE EQUILIBRATING WEAK-STRONG APPROXIMATION

As described above, the strong beam is assumed Gaussian, and its variance in each of 3 dimensions updated to match that of the weak beam as required. If the distribution of the macroparticles of the weak beam remains Gaussian, then the self-consistent weak-strong approxima-

tion is good. A non-Gaussian distribution of the weak beam would tend to undermine its credibility. We define χ^2 of fitted and measured distributions

$$\chi^2 = \sum_{i=1}^{N_{bins}} \left(\frac{n_i - \int_{y_{i-1}}^{y_i} f(y)dy}{\sqrt{n_i}} \right)^2, \qquad (4)$$

where

$$f(y) = \frac{N}{\sigma\sqrt{2\pi}} e^{-y^2/2\sigma^2}, \qquad (5)$$

n_i is the number of macroparticles with y coordinate in the ith bin, and N is the total number of macroparticles. χ^2 per degree of freedom averaged over the last 2×10^4 of 10^5 turns, as a function of bunch current is shown in Fig. 10 for the low energy configuration. The horizontal and longitudinal distributions remain strictly Gaussian to the highest bunch current consistent with good lifetime. The vertical distribution begins to develop non-Gaussian tails at about 1.5 mA/bunch. But even at the highest bunch current with good lifetime as measured in CESR, namely, about 2 mA/bunch at 1.9 GeV beam energy (see Fig. 8), the vertical distribution is reliably represented by a Gaussian ($\chi^2 \sim 1$), and the Bassetti-Erskine formulation of the beam-beam kick remains a good approximation.

VII. LIFETIME

The highest bunch currents for which we have luminosity data, about 9.5 mA at high energy (Fig. 7) and 1.9 mA at low energy (Fig. 8) are the beam-beam limiting currents.

---

[1]We find at low energy that we achieve best lifetime if we leave an ion clearing gap. We operate with the ninth train missing, leaving 8, 5 bunch trains.
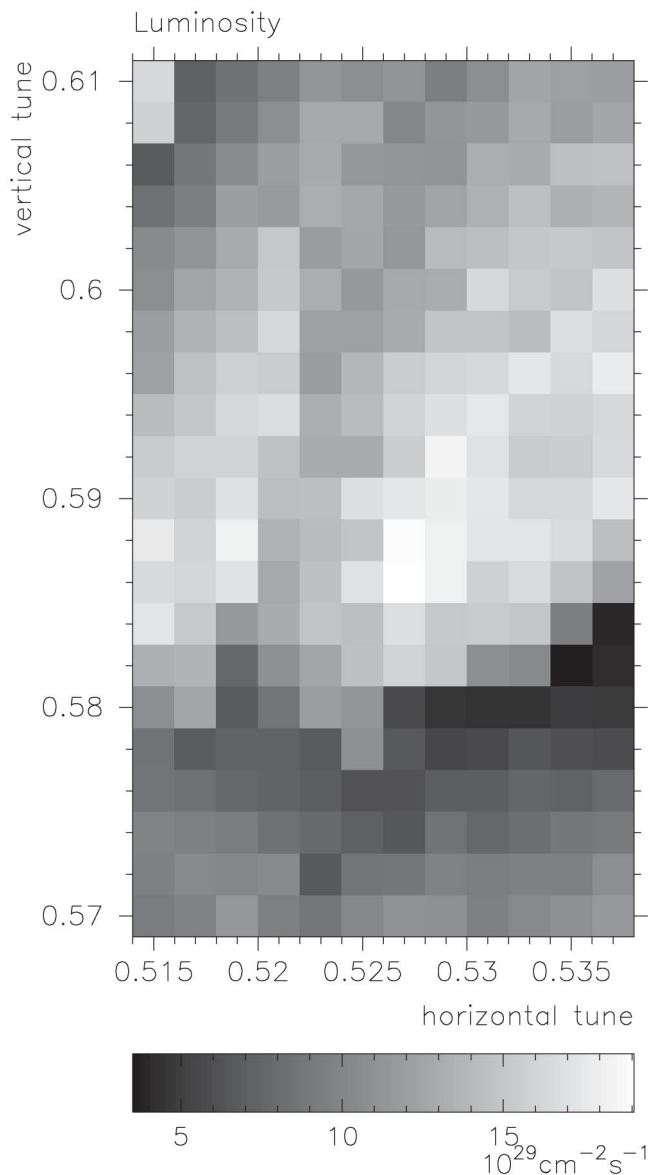
FIG. 9.   Luminosity is computed for each combination of vertical and horizontal tune in the plotted grid. The synchrotron tune is $Q_s = 0.089$. Maximum luminosity occurs for $Q_x = 0.527$ and $Q_y = 0.586$

With further increases in bunch current we measure unacceptably short lifetime (< 30 min).

In the simulation, finite lifetime is indicated if a trajectory falls outside the physical aperture of the machine. If the number of particles N remaining within the machine aperture after time t is $N = N_0 e^{-t/\tau}$. Then

$$\frac{1}{\tau} = \frac{1}{N}\frac{dN}{dt} = \frac{1}{N_{mp}}\frac{\Delta N}{n_t}f_{\text{rev}}, \qquad (6)$$

where N_{mp} is the number of macroparticles, ΔN is the number of macroparticles lost in n_t turns, and f_{rev} is the revolution frequency. In order to explore current depen-

dence of lifetime in the 1.89 GeV configuration, we track 5×10^3 macroparticles for 10^5 turns. Inverse lifetime is shown in Fig. 11. The loss of a single particle is equivalent to a lifetime of about 20 min ($f_{\text{rev}} = 390.1$ kHz). For bunch current less than 2.6 mA, none of the 5×10^3 particles are lost in 10^5 turns and we conclude that lifetime is greater than 20 min (as compared to the measured $\tau \sim$ 40 min at 1.9 mA). Lost particles fall outside the horizontal aperture, which is limited in CESR because of the differential displacement of the closed orbits required to separate counter-rotating beams in the machine arcs. We are exploring the sensitivity of lifetime to the separation amplitude, as well as guide field misalignments and orbit errors.

VIII. TUNE SHIFT PARAMETER

Given the relationship between vertical beam-beam tune shift parameter ξ_v, bunch current, and luminosity,

$$\xi_v = \frac{\beta_v^* L_b}{I_b}\left(\frac{2er_e}{\gamma}\right) \qquad (7)$$

we determine that in the high-energy configuration $\xi_v \sim$ 0.06. However, in the CESR-c low energy configuration, the tune shift saturates at a relatively low value of $\xi_v \sim$ 0.026 at the beam-beam limit of 1.9 mA/bunch. Remember that the simulation and measurement are in good agreement, and the simulation is based on an ideal, error free lattice. We conclude that there is some characteristic fundamental to the CESR-c design that limits beam-beam performance.

We use the simulation to explore sources of the vertical emittance dilution, including long range beam-beam forces, the crossing angle, and wiggler nonlinearities. We find no significant change in current dependence of the tune shift parameter when we eliminate the parasitic crossings and/or the crossing angle and the associated electron positron orbit difference. Similarly, elimination of wiggler nonlinearities has no effect on beam-beam performance

Even at very low current, where beam-beam effects are expected to be negligibly small, the vertical beam size is not. The simulated dependence of vertical beam size on bunch current is shown in Fig. 12. The dilution of the vertical emittance is evidently a single beam effect.

There are two sources of vertical emittance in the CESR-c configuration.

(i) Dispersion generated by the half wave electrostatic vertical bump that separates the electron and positron beams at the crossing point diametrically opposite the interaction point.

(ii) Dispersion generated by the horizontal displacement of the closed orbit in the interaction region quadrupoles which are rotated to compensate for the experimental solenoid.

But we find no significant reduction in vertical beam size in a simulation with all electrostatic separators turned off
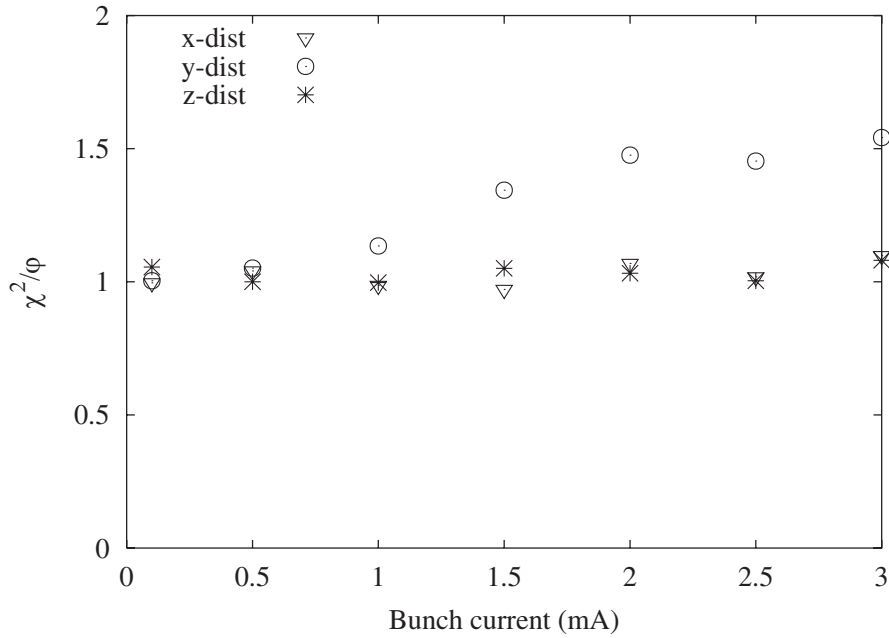
FIG. 10. χ^2 per degree of freedom for fitted Gaussian.

and conclude that the dilution of vertical beam size is not due to vertical dispersion.

IX. SOLENOID COMPENSATION

In CESR-c the 1.0 T field of the CLEO solenoid is compensated with three antisymmetrically placed pairs of skew and rotated quadrupoles. The final focus quadrupoles (one vertically and one horizontally focusing) are rotated by 4.5° about their axes. Superimposed skew quadrupole windings permit fine tuning of the effective rotation angle. The third degree of freedom required to decouple beams at the interaction point is provided by a skew quadrupole located on the interaction region side of the first bending magnet.

The compensation region or insert is defined as the guide field between the bending magnets that surround the IR.
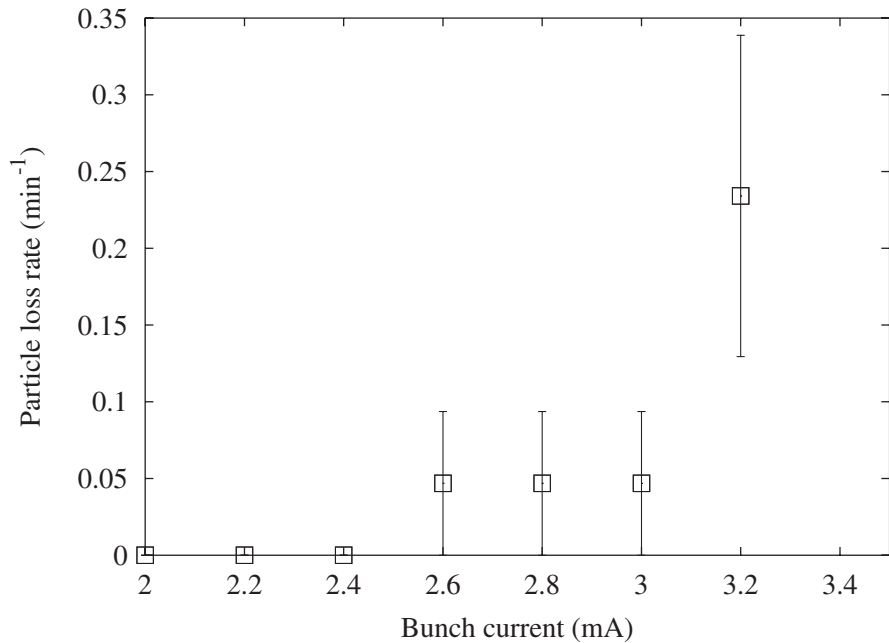

FIG. 11. $1/\tau = (f_{\mathrm{rev}}/N_{mp})(\Delta N/n_t)$. $\Delta N = 0$ for bunch current less than 2.4 mA. The lifetime is about 20 min at 2.6 mA. In CESR we measure a lifetime of about 40 min with an average current of 1.9 mA/bunch.
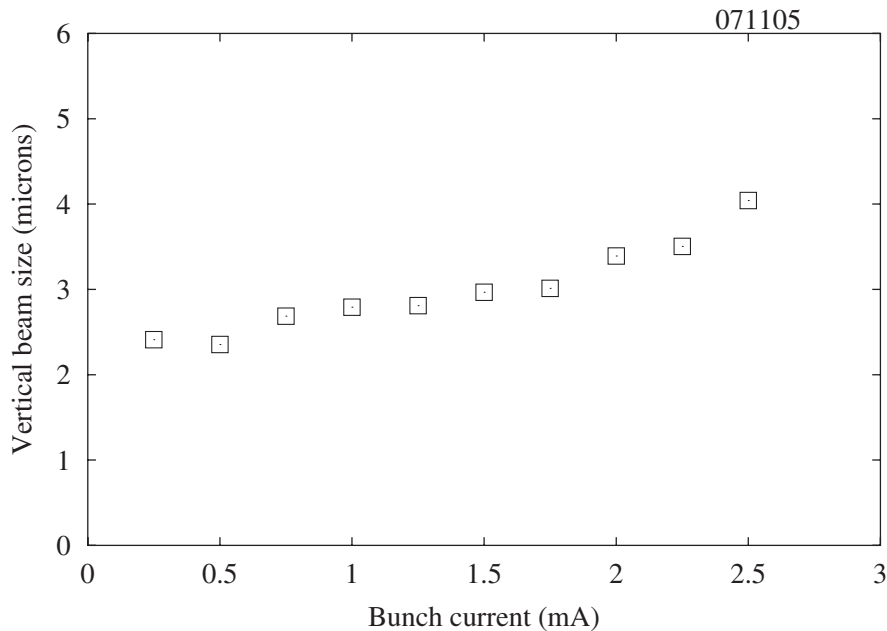
071105

FIG. 12.   Fitted vertical beam size of the weak beam distribution yielding the luminosity displayed in Fig. 8.

Compensation requires that the transfer matrix through the compensation region be block diagonal, and that at the interaction point, three of four elements of the full turn coupling matrix be zero ($\bar{c}_{11} = \bar{c}_{12} = \bar{c}_{21} = 0$), thus ensuring that horizontal motion outside of the compensation region is not coupled to vertical displacement at the interaction point [14]. It is in general not possible to constrain the entire coupling matrix to be zero at the IP with only 3 pairs of skew elements, and there is insufficient phase advance within the compensation region to locate a nondegenerate fourth pair.

The compensation is, by design, perfect for on energy trajectories. We characterize the energy dependence, or chromaticity of the compensation in terms of the energy derivative of coupling parameters at the IP and for the insert. Let **T** represent the 4×4 full turn transfer matrix at the interaction point. Then according to the normal mode decomposition [15],

$$\mathbf{T} = \mathbf{V}\mathbf{U}\mathbf{V}^{-1} \qquad (8)$$

where **U** is block diagonal and

$$\mathbf{V} = \begin{pmatrix} \gamma\mathbf{I} & \mathbf{C} \\ \mathbf{C}^{\dagger} & \gamma\mathbf{I} \end{pmatrix}. \qquad (9)$$

The normalized coupling matrix is

$$\bar{\mathbf{C}} = \mathbf{G}_a\mathbf{C}\mathbf{G}_b^{-}1, \qquad (10)$$

where

$$\mathbf{G}_i = \begin{pmatrix} \frac{1}{\sqrt{\beta_i}} & 0 \\ \frac{\alpha_i}{\sqrt{\beta_i}} & \sqrt{\beta_i} \end{pmatrix}. \qquad (11)$$

For the standard CESR-c optics, with 1 T solenoid we have that

$$\bar{\mathbf{C}} = \begin{pmatrix} 0.0 & 0.0 \\ -0.074 & 0.0 \end{pmatrix} \qquad (12)$$

and

$$\frac{d\bar{\mathbf{C}}}{d(\delta E/E)} = \begin{pmatrix} -1.21 & 1.60 \\ -16.52 & -0.41 \end{pmatrix}. \qquad (13)$$

The chromaticity of the coupling depends on the horizontal and vertical tune split, and the values indicated are meant to be representative.

The energy derivative of the coupling matrix of the insert itself is independent of machine tunes. We define $\mathbf{T}_I$ as the 4×4 matrix through the compensation insert. Then as before, $\mathbf{T}_I = \mathbf{V}_I\mathbf{U}_I\mathbf{V}_I^{-}1$ and

$$\mathbf{V}_I = \begin{pmatrix} \gamma_I\mathbf{I}_I & \mathbf{C}_I \\ \mathbf{C}_I^{\dagger} & \gamma_I\mathbf{I}_I \end{pmatrix}. \qquad (14)$$

By design, $\mathbf{C}_I = 0$. The energy derivative is

$$\frac{d\bar{\mathbf{C}}_I}{d(\delta E/E)} = \begin{pmatrix} -1.36 & -862.6 \\ 0.10 & -58.71 \end{pmatrix}. \qquad (15)$$

It is clear that the energy dependence of the compensation insert is nonnegligible.

If the low current vertical beam size (as shown in Fig. 12) is due to the solenoid and related compensation, then optics in which the solenoid and its compensation are eliminated will yield reduced beam size and higher luminosity. In order to test the hypothesis, we design interaction region optics in which the solenoid is turned off, the rotated quads are leveled and the strengths of the skew quadru-
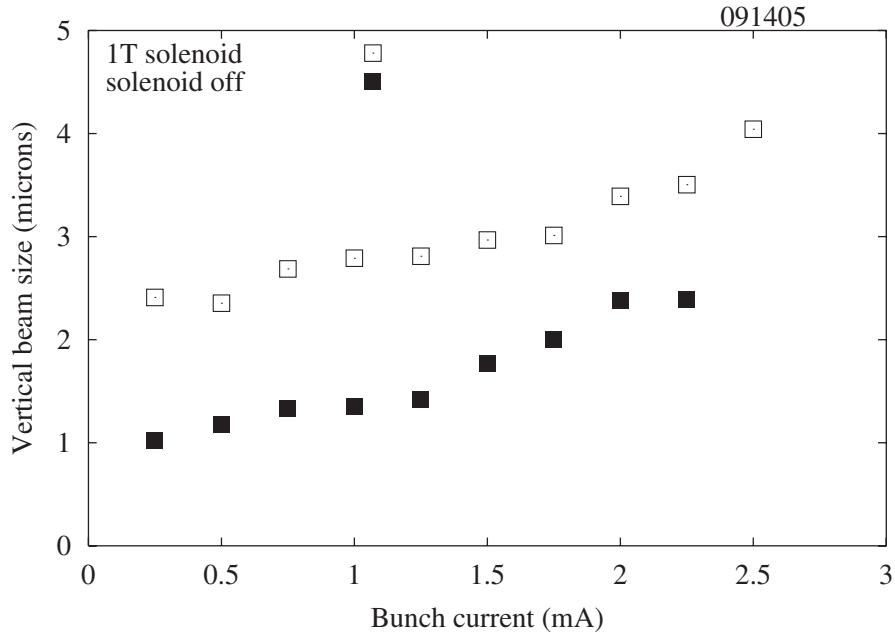
FIG. 13.   Fitted vertical beam size for the solenoid off optics and standard cesr-c optics with 1 T solenoid.

poles set to zero. The results of the simulation of beam size and luminosity for the test optics with no experimental solenoid are shown in Figs. 13 and 14.

We see that the solenoid compensation nearly doubles the low current beam size. Elimination of the solenoid yields a nearly 50% increase in specific luminosity at 2 mA/bunch. In CESR-c we are especially sensitive to the chromaticity of the compensation because the energy spread in the beam is relatively high. The CESR operations group is planning to install antisolenoids in the interaction region to reduce the energy dependence of the compensation and shrink the zero current beam size.

X. BUNCH LENGTH AND SYNCHROTRON TUNE

Another effect of the large energy spread in CESR-c is that a relatively high synchrotron tune is required to maintain a sufficiently short bunch, ($\sigma_l \lesssim \beta_v^*$). With 12, 2.1 T wigglers at 1.89 GeV beam energy, the fractional energy spread is $\sigma_E/E = 8.4 \times 10^{-4}$. The bunch length is
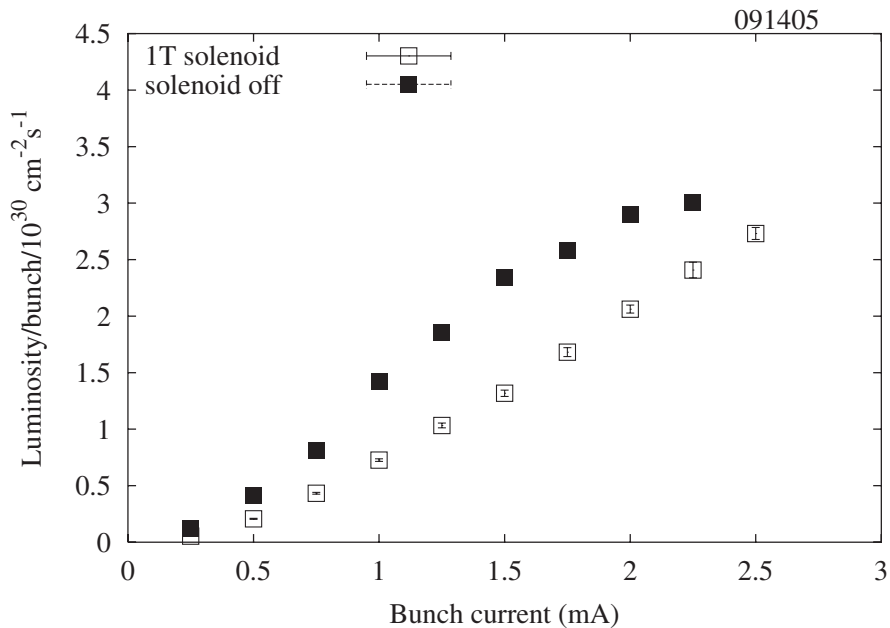

FIG. 14.   Simulated luminosity for the solenoid off optics and standard cesr-c optics with 1 T solenoid.
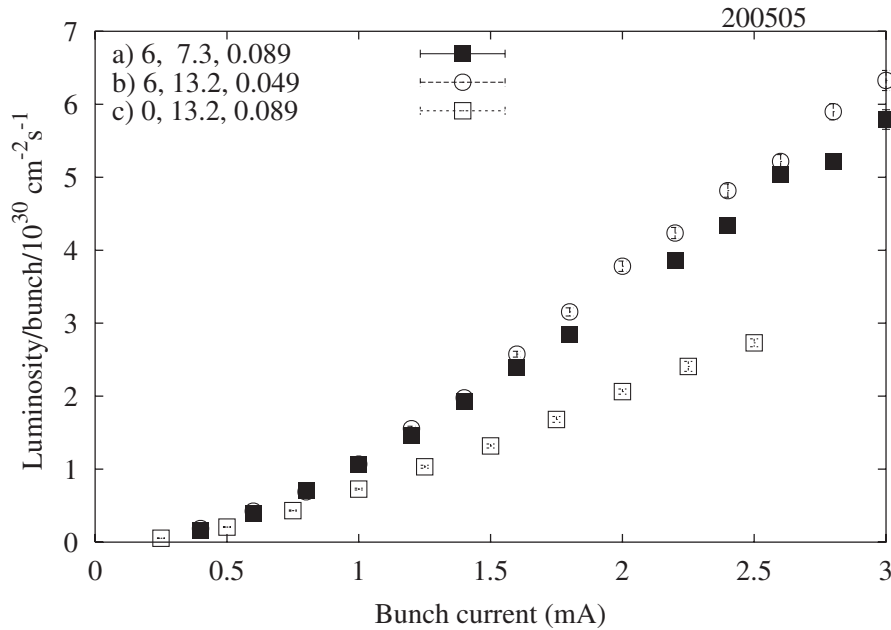
FIG. 15.   Simulated luminosity for the CESR-*c* optics with (a) $M_{56} = 6$ m with high Q_s and short bunch ($Q_s = 0.089$ and $\sigma_l = 7.3$ mm), (b) $M_{56} = 6$ m with low Q_s and long bunch, ($Q_s = 0.049$ and $\sigma_l = 13.2$ mm), and (c) standard CESR-*c* optics, $M_{56} = 0$, ($Q_s = 0.089$ and $\sigma_l = 13.2$ mm).

13.2 mm when the synchrotron tune is $Q_s = 0.089$. (Note that $\beta_v^* = 12$ mm and $\alpha_p = 0.0113$.) In order to explore dependence of luminosity on synchrotron tune and bunch length, we introduce an element into the lattice that will artificially reduce momentum compaction. The element **M** is represented by a 6×6 matrix. The only nonzero off diagonal component is M_{56}. The diagonal components are

unity. The effect of element *M* is to change the relationship between bunch length and synchrotron tune. We choose $M_{56} = 6$ m so that $Q_s = 0.049$ corresponds to a bunch length of 13.2 mm or alternatively so that $Q_s = 0.089$ gives a bunch of length 7.3 mm. The results of the simulation are shown in Figs. 15 and 16. Reduction of the geometric mean of bunch length and synchrotron tune by
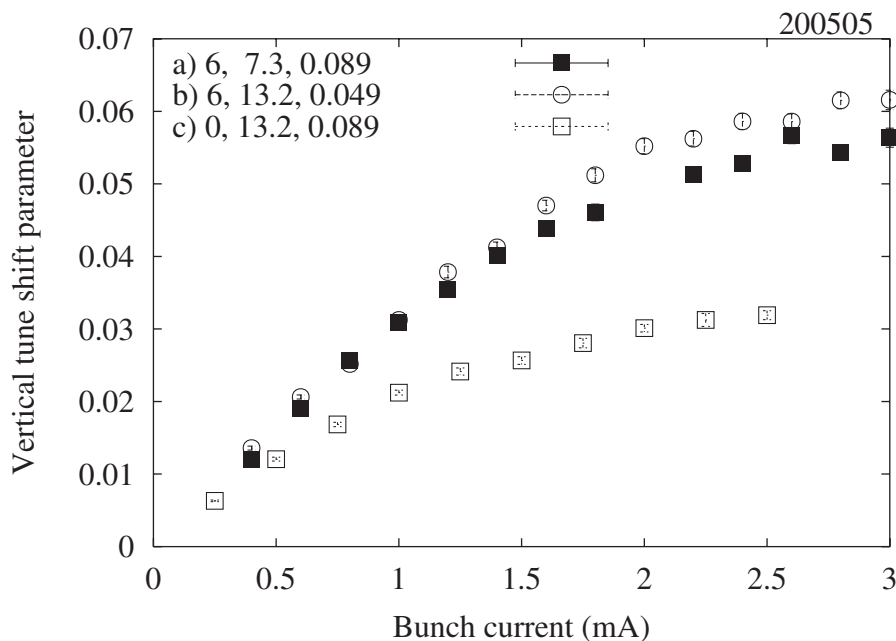

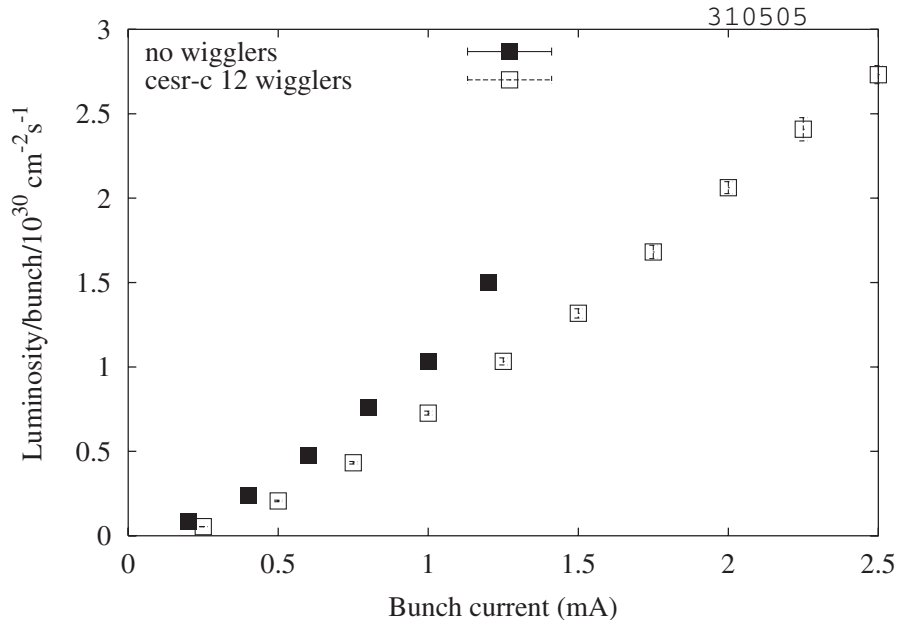FIG. 16.   Beam-beam tune shift corresponding to luminosity shown in Fig. 15.

FIG. 17.   Simulated luminosity for the 1.89 GeV/beam optics with no damping wigglers. The simulated luminosity data for standard CESR-*c* optics are plotted for reference.

75% yields a near doubling of the beam-beam tune shift at the bunch current limit of 2 mA. Within the statistical error of the simulation, and to the extent that the weak-strong approximation continues to be valid with increasing beam-beam tune shift, we find that shrinking the length of the bunch and reducing the synchrotron tune are roughly equivalent.

XI. DAMPING DECREMENT

The damping wigglers were installed in the storage ring to reduce the radiation damping time (damping decrement) at 1.89 GeV beam energy by a factor of 10 from 0.5 s to 50 ms, and to increase horizontal emittance from 20 nm to about 130 nm. An unavoidable side effect is the four fold increase in fractional energy spread. Without the wigglers, there is no degradation of vertical beam size due to energy dependence of the solenoid compensation, and short bunch and low synchrotron tune are no longer mutually exclusive. The parameters of the low energy (1.89 GeV/beam) optics with no damping wigglers are summarized in Table I. The results of the simulation of luminosity versus bunch current are shown in Fig. 17. As before we track for 5 damping times, which in the case of the no wiggler configuration, is about 10^6 turns. Specific luminosity, at bunch current below 1.4 mA, is significantly higher in the wiggler off optics than in standard CESR-*c* conditions with 12 2.1 T damping wigglers. Bunch current is limited to less than 1.4 mA by particle loss. The current limit is likely due to the very small horizontal emittance. But we find that the specific luminosity is not degraded by the tenfold decrease in the damping decrement.

Damping wigglers are critical to the operation of CESR-*c*. The injection rate and multibunch instability thresholds scale roughly linearly with radiation damping rate, and the wigglers provide a mechanism for establishing reasonable emittance [9]. However, the simulation indicates that there is little effect on achievable beam-beam tune shift.

XII. CONCLUSIONS

A weak-strong beam-beam simulation that includes transport through an element by element representation of the machine arcs is in good agreement with CESR luminosity measured at both 5.289 GeV beam energy and 1.89 GeV beam energy. There are no adjustable parameters in the simulation. The validity of the weak-strong approximation and the assumption of Gaussian particle distribution begins to break down only as the bunch current approaches the measured beam-beam limiting current. With the simulation we find that the energy dependence of the compensation of the experimental solenoid dilutes vertical beam size and degrades luminosity at low bunch current. We are planning to install antisolenoids in the CESR-*c* interaction region to reduce the energy dependence as has been done at the DAFNE [16] collider. The simulation also indicates that the high synchrotron tune required to maintain bunch length no greater than β_v^* in CESR-*c*, limits the beam-beam tune shift.

———————

[1] D. Rubin *et al.*, in *Proceedings of the Particle Accelerator Conference, Chicago, IL, 2001* (IEEE, Piscataway, 2001), p. 3520.

[2] J. Crittenden *et al.*, in *Proceedings of the Particle Accelerator Conference, Portland, OR, 2003* (IEEE, Piscataway, 2003), p. 1023.

[3] D. Sagan, http://www.lns.cornell.edu/~dcs/bmad/

[4] G. Jackson and R. Siemann, Nucl. Instrum. Methods Phys. Res., Sect. A **286**, 17 (1990).

[5] S. Krishnagopal and R. Siemann, Phys. Rev. D **41**, 2312 (1990).

[6] K. Ohmi, M. Tawada, Y. Cai, S. Kamada, K. Oide, and J. Qiang, Phys. Rev. Lett. **92**, 214801 (2004).

[7] E. B. Anderson, T. I. Banks, and J. T. Rogers, in *Proceedings of the Particle Accelerator Conference, New York, 1999* (IEEE, Piscataway, 1999), pp. 1686–1688.

[8] J. Sikora, Report No. CESR ELOG 2002-03-05.

[9] D. Rice *et al.*, in *Proceedings of the Particle Accelerator Conference, Chicago, IL, 2001* (Ref. [1]), p. 374.

[10] M. Sands, Report No. SLAC-121, 1970, pp. 118–120.

[11] R. Talman, in *Physics of Particle Accelerators*, AIP Conf. Proc. No. 153 (AIP, New York, 1987), p. 789.

[12] D. Rubin and D. Sagan, in *Proceedings of the Particle Accelerator Conference, Portland, OR, 2003* (Ref. [2]), p. 777.

[13] S. Henderson *et al.*, in *Proceedings of the Particle Accelerator Conference, New York, 1999* (Ref. [7]), p. 3221.

[14] *Handbook of Accelerator Physics and Engineering*, edited by A. Chao and M. Tigner (World Scientific, River Edge, NJ, 1999).

[15] D. Sagan and D. Rubin, Phys. Rev. ST Accel. Beams **2**, 074001 (1999).

[16] *Proceedings of the Advanced ICFA Beam Dynamics Workshop*, edited by L. Palumbo and G. Vignola, Frascati Physics Series X (Instituto Nazionale de Fisica Nucleare, Frascati, 1997).